© 2026 Journal of Pharmacy & Pharmacognosy Research, 14 (2), 2272, 2026
ISSN 0719-4250
https://jppres.com

DOI: https://doi.org/10.56499/jppres_14.2.2272

Original Article

Identifying high-efficiency α-glucosidase inhibitors from *Abelmoschus manihot* (L.) Medik.: A quadrant-based integration of *in vitro* potency and *in silico* analysis

[Identificación de inhibidores de α-glucosidasa de alta eficiencia en *Abelmoschus manihot* (L.) Medik.: una integración basada en cuadrantes de potencia *in vitro* y análisis *in silico*]

Juliet Tangka[1], Jovie M. Dumanauw[1], Nurdiana[2], Rudy Salam[3], Diana Lyrawati[3*]

[1]Department of Pharmacy, Manado Health Polytechnic, Ministry of Health, Manado, Indonesia.
[2]Department of Pharmacology, Faculty of Medicine, Universitas Brawijaya, Malang, Indonesia.
[3]Department of Pharmacy, Faculty of Medicine, Universitas Brawijaya, Malang, Indonesia.
*E-mail: diana.l@ub.ac.id

Abstract

Context: α-Glucosidase represents one of the key treatments for diabetes based on its ability to regulate postprandial blood glucose levels.

Aims: To evaluate the α-glucosidase inhibitory potential of *Abelmoschus manihot* (L.) Medik, an endemic species of Minahasa, Indonesia, which is consumed as a vegetable and has been used as an anti-diabetic herbal medicine.

Methods: The α-glucosidase inhibitory activity of *A. manihot* ethanolic extract was benchmarked against acarbose *in vitro*. A multi-parametric quadrant analysis was applied to 27 identified phytochemicals to rank them based on binding affinity (ΔG) and ligand efficiency (LE). Top-ranked leads (stigmasterol and hibiscone-B) underwent 100 ns molecular dynamics (MD) simulations and MM-PBSA calculations to validate binding stability and energetic profiles.

Results: The extract demonstrated robust, dose-dependent inhibition (IC_{50} = 1069.71 µg/mL) and achieved superior maximal efficacy (92.0%) compared to acarbose. Quadrant analysis identified stigmasterol as a "Power Binder" (ΔG = -9.17 kcal/mol) and hibiscone-B as a "Precision Lead" (LE = -0.43), both of which outperformed acarbose in atomic binding efficiency. MD simulations confirmed that hibiscone-B maintains a stable occupancy of the catalytic cleft, supported by persistent hydrogen bonds with ASP203 and ASP542.

Conclusions: *A. manihot* serves as a potent botanical matrix for anti-diabetic leads. The narrow 3.5-fold potency gap between the crude extract and its pure lead, hibiscone-B, underscores the high efficiency of its phytochemical components, offering a superior alternative to traditional carbohydrate-mimetic inhibitors. Hibiscone-B and stigmasterol are identified as high-priority templates for the development of next-generation inhibitors.

Keywords: *Abelmoschus manihot*; α-glucosidase; hibiscone-B; molecular dynamics; stigmasterol; type 2 diabetes.

Resumen

Contexto: La α-glucosidasa representa uno de los tratamientos clave para la diabetes debido a su capacidad para regular los niveles de glucosa en sangre posprandial.

Objetivos: Evaluar el potencial inhibidor de la α-glucosidasa de *Abelmoschus manihot* (L.) Medik, una especie endémica de Minahasa, Indonesia, que se consume como verdura y se ha utilizado como medicina herbal antidiabética.

Métodos: La actividad inhibidora de la α-glucosidasa del extracto etanólico de *A. manihot* se comparó con la de la acarbosa *in vitro*. Se aplicó un análisis de cuadrantes multiparamétrico a 27 fitoquímicos identificados para clasificarlos según su afinidad de unión (ΔG) y eficiencia del ligando (LE). Los compuestos principales (estigmasterol e hibiscona-B) se sometieron a simulaciones de dinámica molecular (DM) de 100 ns y cálculos MM-PBSA para validar la estabilidad de la unión y los perfiles energéticos.

Resultados: El extracto demostró una inhibición robusta y dependiente de la dosis (CI_{50} = 1069,71 µg/mL) y alcanzó una eficacia máxima superior (92,0 %) en comparación con la acarbosa. El análisis de cuadrantes identificó al estigmasterol como un "ligando potente" (ΔG = -9,17 kcal/mol) y a la hibiscona-B como un "compuesto principal de precisión" (LE = -0,43), ambos con una eficiencia de unión atómica superior a la de la acarbosa. Las simulaciones de dinámica molecular confirmaron que la hibiscona-B mantiene una ocupación estable de la hendidura catalítica, respaldada por enlaces de hidrógeno persistentes con ASP203 y ASP542.

Conclusiones: *A. manihot* constituye una matriz botánica potente para compuestos principales antidiabéticos. La estrecha diferencia de potencia de 3,5 veces entre el extracto crudo y su compuesto principal puro, la hibiscona-B, subraya la alta eficacia de sus componentes fitoquímicos, ofreciendo una alternativa superior a los inhibidores tradicionales que imitan los carbohidratos. La hibiscona-B y el estigmasterol se han identificado como modelos prioritarios para el desarrollo de inhibidores de próxima generación.

Palabras Clave: *Abelmoschus manihot*; diabetes tipo 2; dinámica molecular; estigmasterol; α-glucosidasa; hibiscona-B.

ARTICLE INFO
Received: November 20, 2024.
Accepted: March 24, 2026.
Available Online: April 9, 2026.

AUTHOR INFO
ORCID: 0000-0003-1355-3133 (JT) 0009-0005-5879-5752 (RS)
0000-0003-4042-6375 (JMD) 0000-0001-5931-3245 (DL)
0000-0002-7953-1124 (N)

INTRODUCTION

Type 2 diabetes mellitus (T2DM), a chronic metabolic disease, is characterized by hyperglycemia and an imbalance between insulin secretion and insulin sensitivity (DeFronzo et al., 2015; Khan et al., 2020). α-Glucosidase inhibitors represent one drug class used to manage T2DM. The clinically available α-glucosidase inhibitors used to treat diabetes, namely, acarbose, voglibose, and miglitol, competitively inhibit α-glucosidase in the small intestine and consequently delay the hydrolysis of carbohydrates (starch and disaccharides), thereby reducing postprandial hyperglycemia (Guo et al., 2015; Gupta et al., 2016).

While current α-glucosidase inhibitors effectively manage postprandial blood sugar levels, their use is hampered by several limitations, including gastrointestinal adverse effects, which led to patient non-adherence (Fisher, 2022). Thus, new α-glucosidase inhibitors are actively being pursued. Compounds from functional foods widely used to treat T2DM are critical to the search for new anti-diabetics because they reduce postprandial hyperglycemia with few gastrointestinal side effects. The leaves of *Abelmoschus manihot* (L.) Medik (family *Malvaceae*), a species endemic to Minahasa, North Sulawesi, Indonesia, that is also known as red gedi, has been consumed as a vegetable and is widely used as an anti-diabetic herbal medicine (Nurrani & Kinho, 2013; Suoth et al., 2013). Our previous study identified 38 metabolites in the ethanolic extract of this plant (Tangka et al., 2021). To date, few studies have investigated the anti-diabetic pharmacology of the extract and its components (Fitriyah et al., 2020; Fuadi et al., 2020; Nurasidah et al., 2020; Sakinah et al., 2020).

In this study, the α-glucosidase–inhibitory activity of *A. manihot* leaf extract was determined using *in vitro* assays, and the metabolites were analyzed using *in silico* molecular docking to predict which metabolites contributed to this activity. Identified phytochemicals serve as templates or lead compounds that can be further optimized to yield novel, safe, and effective drugs. Computational molecular simulation or virtual screening aims to identify new drug candidates by docking large libraries of small molecules into the binding site of the therapeutic target and using scoring functions to determine binding poses and estimate binding affinity (Agu et al., 2023). Such *in silico* studies can predict the binding affinity and selectivity of small molecules, as well as their binding stability with molecular targets, which are important parameters in drug discovery and design (Cole et al., 2019).

MATERIAL AND METHODS

Plant material

The leaves of *A. manihot* were collected from North Tondano Plantation, North Sulawesi, Indonesia (1.30198° N latitude and 124.913399° E longitude). Plant identification was performed at the Center for Plant Conservation Botanic Gardens, Indonesian Institute of Sciences (Bogor, Indonesia, Letter B-3177/IPH.3/KS/IX/2018) (Tangka et al., 2021).

Chemicals

p-Nitrophenyl-α-d-glucopyranoside (PNPG), phosphate buffer, sodium carbonate, α-glucosidase (derived from *Saccharomyces cerevisiae*), and the standard inhibitor acarbose were all of analytical quality and obtained from Sigma-Aldrich (St. Louis, MO, USA).

Extraction

The ethanolic extract of *A. manihot* leaves was generated as previously described (Tangka et al., 2022). Dried *A. manihot* leaves (50 g) were dynamically macerated in 500 mL of 96% ethanol solvent (1:10) and stirred at 30–40°C and 200 rpm for 6 h. The macerate was subsequently evaporated at 50 and 80°C. The final thick extract (12.1 g) was used in α-glucosidase inhibition assays or stored in a refrigerator. Characterization of the compounds in the ethanolic extract of red leaves *A. manihot* was conducted as previously described (Tangka et al., 2021) using a UHPLC system connected to a triple quadrupole mass spectrometer (LCMS-8040; Shimadzu, Kyoto, Japan). Mass spectra were simultaneously acquired using electrospray ionization (ESI) in the positive ionization modes, and full-scan mass spectra were acquired at a mass-to-charge ratio (m/z) of 50–1000.

In vitro α-glucosidase inhibition assay

The α-glucosidase inhibition assay was performed using 96-well ELISA plates (Hamza et al., 2015). In each well, 10 µL of *A. manihot* extract (312.5, 625, 1250, 2500, 5000, and 10,000 µg/mL) or acarbose (3.125, 6.25, 12.5, 25, 50, and 100 µg/mL) were added. The samples in each well were mixed with phosphate buffer (490 µL, 100 mmol/L, pH 7), and PNPG substrate (250 µL, 3 mmol/L) was then added. The plate was incubated at 37°C for 5 min, after which α-glucosidase (250 µL, 0.065 U/mL) was added, and the plate was further incubated at 37°C for 15 min. The reaction was stopped by adding 1000 µL of 0.2 mol/L Na_2CO_3. The nonenzymatic hydrolysis of each substrate was corrected by measuring the increase in absorbance at 405 nm for the control mixture without α-glucosidase. The α-

glucosidase–inhibitory activity of each sample was calculated using Equation [1].

$$\text{Inhibition ratio (\%)} = \frac{1 - [\text{sample OD} - \text{blank 2 OD}]}{[\text{control OD} - \text{blank 1 OD}]} \times 100 \quad [1]$$

For *in vitro* experiments, all analyses were performed in quadruplicate. To calculate the IC_{50}, a logarithmic transformation was employed for the independent variable (concentration) to linearize the dose-response relationship. The logarithmic regression equation was then used to predict the IC_{50}, as it was a superior fit compared to the standard linear model. To ensure comparability between experimental sets and account for inherent assay variability, the inhibitory potential was expressed as a potency ratio (PR), defined as the IC_{50} of the reference standard (acarbose) divided by the IC_{50} of the test sample. This normalization facilitated direct comparison of the crude extract's efficacy with pure phytochemical standards reported in the literature (Finney, 1978).

Statistical analysis

Data from the *in vitro* α-glucosidase inhibition assay were presented as mean ± standard deviation percentages for each concentration tested. To determine the concentration-dependent effect of the ethanolic extract and acarbose, the data were subjected to one-way analysis of variance (ANOVA). Statistical significance was set at $p<0.05$. The IC_{50} values were calculated using nonlinear regression analysis of the dose-response curves. The relationship between concentration and inhibition was modeled using the log-linear equation. All calculations were performed using SPSSv6 (IBM, Armonk, NY, USA).

Computational analysis

The computational workflow was executed in two distinct phases to ensure the reliability of lead identification. In Phase I, molecular docking was used to generate a docking score, which represents a static interaction in a vacuum and served as a rapid heuristic for the initial ranking and bivariate quadrant analysis of the 27 identified phytochemicals. Phase II involved 100 ns molecular dynamics (MD) simulations to calculate the structural persistence and estimate the binding free energy (ΔG) in an explicit aqueous environment. This dual-layer validation ensures that the prioritized leads possess high geometric complementarity and a favorable energetic profile for sustained enzymatic blockade.

Molecular docking

The interaction between bioactive compounds from *A. manihot* leaf extract and the enzyme α-glucosidase was analyzed using molecular docking to evaluate potential inhibitory activity *in silico*. The crystal structure of the N-terminal subunit of human maltase-glucoamylase in complex with acarbose (ID 2QMJ), as determined by X-ray diffraction at 2.45 Å, was collected from the PDB database (https://www.rcsb.org/). The acarbose binding sites identified on the target protein were used as the standard for docking analyses. The 3D ligand structures and 26 identified compounds of A. manihot (Table 1) were collected from the PubChem database (https://pubchem.ncbi.nlm.nih.gov/) in SDF format (Suoth et al., 2013; Tangka et al., 2022). After optimization in Avogadro using hydrogen atoms at pH 7.4, followed by energy minimization by means of the MMFF94 method (Hanwell et al., 2012), all were saved in mol2 format. The next step was ligand preparation for docking using prepare_ligand4.py, which included adding Gasteiger charges, torsions, and converting to PDBQT format. The docking process was performed using AutoDock Vina 1.1.2 with a 35 × 35 Å grid centered on acarbose as the reference ligand, with coordinates -20.81 × -6.58 × -5.07 (Trott & Olson, 2010). To avoid bias due to the large differences in molecular size between compounds (number of heavy atoms 9–44), Ligand Efficiency (LE) was calculated as a parameter for normalizing binding energy per heavy atom using the Equation [2].

$$LE = \frac{E_{binding}}{N_{heavy\ atom}} \quad [2]$$

where $E_{binding}$ was the docking score (kcal/mol), and $N_{heavy\ atom}$ was the number of non-hydrogen atoms (Abad-Zapatero & Metz, 2005; Hopkins et al., 2004).

An LE value ≤ −0.40 is used as the minimum threshold to identify ligands with good binding efficiency and significant inhibitory potential against the target enzyme. Candidate ligands that meet these criteria proceed to molecular interaction analysis using Chimera 1.15 and Discovery Studio Visualizer 2020 (Dassault, 2020). Of the 38 phytochemicals previously reported (Tangka et al., 2021), 26 were used in molecular docking. The other 12 phytochemicals were excluded: 8 of them are glycoside compounds (where the alkaloid component was already included in the first 26 compounds), and the remaining 4 were unlikely to enter the bloodstream due to their molecular size (> 500 Da). Candidate ligands with interaction patterns similar to those of acarbose at the alpha-glucosidase binding site are subjected to molecular dynamics simulations to assess the stability of their interactions.

Multi-parametric prioritization and quadrant analysis

To move beyond raw binding energies and identify the most biologically relevant inhibitors, a multi-parametric prioritization strategy was employed.

Table 1. Docking scores and ligand efficiency (LE) of *A. manihot* compounds.

Ligand	Heavy atom	Docking score (ΔG, kcal/mL)	LE
Acarbose (reference drug)	44	-7.17	-0.16
Alpha-spinasterol	30	-8.87	-0.30
Aquillochin acid	30	-6.73	-0.22
Caffeic acid methyl ester	14	-6.20	-0.44
Cis-P-coumaric acid	12	-5.93	-0.49
Cyanidin	21	-7.40	-0.35
Daphniphyllin	38	-7.03	-0.19
Farnesol	16	-6.10	-0.38
Ferulic acid	14	-5.90	-0.42
Ficusol	16	-5.63	-0.35
Gmelofuran	18	-6.80	-0.38
Gossypetin	23	-7.67	-0.33
Hibiscetin	24	-7.80	-0.33
Hibiscone-A	17	-6.47	-0.38
Hibiscone-B	17	-7.27	-0.43
Hibiscoquinone-A	19	-7.00	-0.37
Kaempferol	21	-7.40	-0.35
Malic acid	9	-4.70	-0.52
Moupinamide	23	-7.33	-0.32
Myricerol	23	-7.57	-0.33
Myricetin	23	-7.60	-0.33
Quercetin	22	-7.50	-0.34
Stigmasterol	30	-9.17	-0.31
Syringaresinol	30	-6.60	-0.22
Syringic acid	14	-5.00	-0.36
Trans-P-coumaric acid	23	-7.03	-0.31
Vanillic acid	12	-5.40	-0.45

The 27 phytochemicals were analyzed using a Quadrant Analysis framework, which integrated binding affinity (ΔG) and ligand efficiency (LE). Threshold setting: a stringent high-affinity threshold was set at ΔG≤-7.5 kcal/mol, and a high-efficiency threshold was set at LE ≤-0.40 kcal/mol/heavy atom. Compounds were mapped onto a master correlation plot, with the X-axis representing binding affinity (ΔG) and the Y-axis representing ligand efficiency (LE). Categorization: based on these thresholds, ligands were divided into four distinct functional quadrants: Q1 (the elite performers): compounds meeting both stringent thresholds (ΔG ≤-7.5 and LE ≤-0.40); Q2 (The Precision Fragments): high efficiency (LE ≤-0.40) despite moderate raw affinity; Q3 (the low-priority binders): compounds failing both thresholds; and Q4 (the bulky/power binders): high affinity (ΔG ≤-7.5) but lower atomic efficiency (LE > -0.40).

Molecular dynamics (MD) simulation

All MD simulations were performed using GROMACS version 2025 with a simulation period of 100 ns (Van Der Spoel et al., 2005). The protein and ligand topologies were prepared in advance; the protein topology was obtained by applying the all-atom CHARMM36 force field (Huang & MacKerell, 2013), and the ligand topology files were generated by adding hydrogen atoms using Avogadro (Hanwell et al., 2012) and submitting them to the CgenFF web server (Vanommeslaeghe et al., 2012). All complexes were dissolved in a dodecahedron box containing TIP3P water and chloride ions to neutralize the system,

maintaining a minimum distance of 1 Å between the box edge and the protein. Energy minimization was then applied to the system using the Verlet cutoff scheme, resulting in a maximum force of <10 kJ/mol/nm over up to 50,000 steps, while eliminating unwanted steric clashes and poor contacts. Equilibration was performed in the canonical (NVT) and isothermal-isobaric (NPT) ensembles. The NVT equilibration step was carried out at a constant volume at 300 K using the modified Berendsen thermostat algorithm for 1000 ps. Next, NPT equilibration was performed at a constant pressure of 1 bar and 300 K using the Parrinello–Rahman barostat for 1000 ps. Subsequently, a 100 ns production simulation (NPT) was performed, and the MD results were analyzed using scripts integrated into the GROMACS software package. gmx rms and gmx hbond were used to determine the RMSD and hydrogen bond parameters throughout the simulation. Hydrogen bond persistence was monitored throughout the 100 ns trajectory using a geometric criterion: a donor–acceptor distance cutoff of 3.5 Å and a bond angle cutoff of 30° (Hubbard & Haider, 2010). To assess the localized flexibility of the enzyme upon ligand binding, the root mean square fluctuation (RMSF) of the Cα atoms was calculated relative to the initial structure. This analysis identifies regions of high mobility (loops) and areas of localized stability (active site), providing insight into the rigidification of the catalytic dyad during the simulation (Abraham et al., 2015). Graphs were processed using QtGrace (https://sourceforge.net/projects/qtgrace/).

The binding free energy (ΔGtotal) of the prioritized lead complexes was calculated using the Molecular Mechanics Poisson-Boltzmann Surface Area (MM-PBSA) method via the g_mmpbsa tool (Kumari et al., 2014). This approach integrates the molecular mechanics energy with the Poisson–Boltzmann (PB) equation for polar solvation and the solvent-accessible surface area (SASA) for non-polar solvation contributions, excluding the entropic term, as per standard protocols for relative binding affinity ranking (Genheden & Ryde, 2015). For each system, 100 snapshots were extracted from the last 20 ns of the stable MD trajectory to ensure that the system had reached energetic equilibrium. The total binding energy was deconvoluted into its components according to Equation [3].

$$\Delta Gbind = \Delta EMM + \Delta Gsolv - T\Delta S \quad [3]$$

The vacuum molecular mechanics potential (ΔEMM) included both electrostatic and van der Waals interactions. The solvation free energy (ΔGsolv) was estimated using a **d**ielectric constant of 80 for the solvent and 2 for the protein interior. The non-polar solvation contribution was calculated based on the solvent-accessible surface area (SASA) with a surface tension coefficient (γ) of 0.02267 kJ/mol/Å^2. Owing to the high computational demand and relative nature of the study, the configurational entropy contribution (–TΔGS) was not included, and the results are reported as relative binding affinities.

RESULTS

In vitro assay

The ethanolic extract of *A. manihot* leaves was investigated for α-glucosidase inhibitory activity using *in vitro* assays. Acarbose was used as the standard for comparison. The experiments were replicated four times. Both the ethanolic extract and acarbose exhibited potent, dose-dependent inhibition of α-glucosidase (Table 2). The inhibitory activity increased significantly with higher concentrations ($p<0.001$).

Table 2. α-Glucosidase–inhibitory effects of *A. manihot* leaf ethanolic extract

Ethanolic extract of *A. manihot* leaves			**Acarbose**		
Concentration (µg/mL)	**Maximum inhibition [mean ± SD (%)], (n = 4)**	**p-value**	**Concentration (µg/mL)**	**Maximum inhibition [mean ± SD (%)], (n = 4)**	**p-value**
312.5	24 ± 0.0153	0.00007	3.125	7 ± 0.0359	0.00009
625	40 ± 0.0082		6.25	8 ± 0.0391	
1250	50 ± 0.0048		12.5	13 ± 0.03623	
2500	72 ± 0.0005		25	16 ± 0.0479	
5000	83 ± 0.0010		50	19 ± 0.0542	
10,000	92 ± 0.0060		100	22 ± 0.0577	
Calc.IC_{50} 1069.71	Equation: $y = 46.6019 \log_{10}(x) - 91.1695$, R^2=0.9860		Calc.IC_{50} 456.24	Equation: $y = 10.4578 \log_{10}(x) + 1.2588$, R^2= 0.9677	

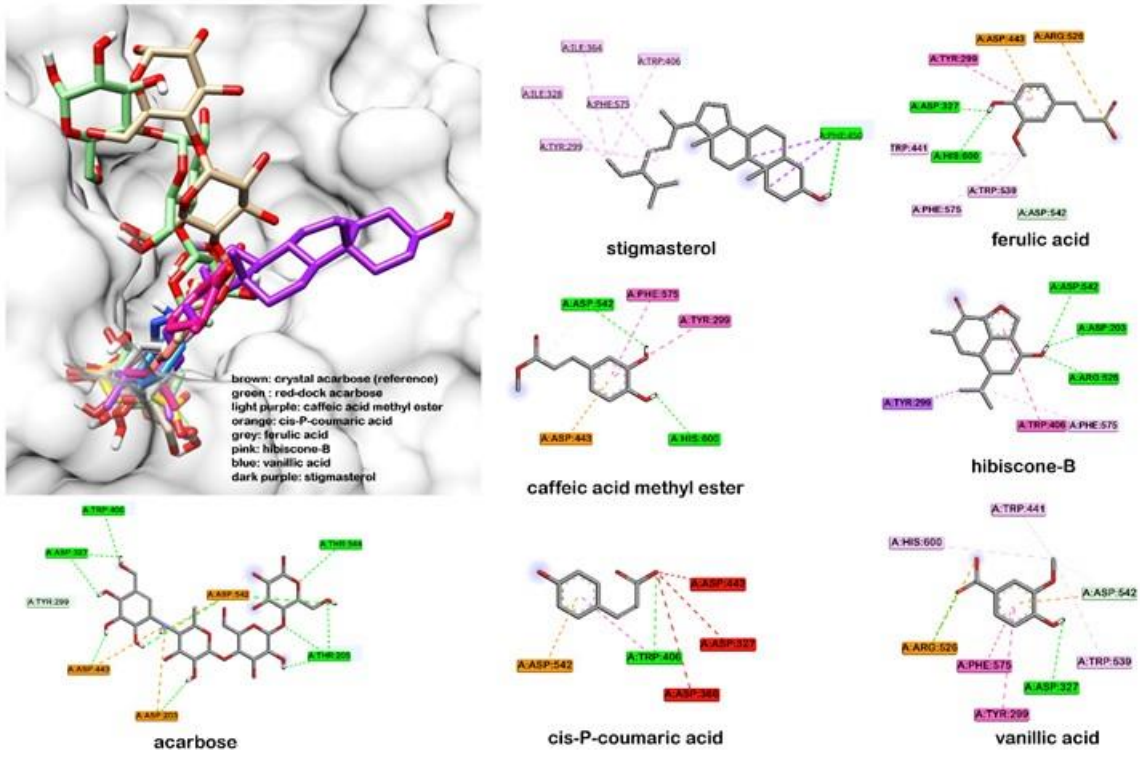


Figure 1. 3D pose at the active site of α-glucosidase and molecular interaction diagram showing interactions between candidate compounds and α-glucosidase.

Statistical significance was assessed using log-linear regression analysis. Logarithmic transformation of the independent variable (concentration) was employed to linearize the dose-response relationship. The regression model showed an excellent fit to the experimental data, with an R^2 coefficient > 0.95. The extract also exhibited a steeper dose-response slope (46.60) compared to that of acarbose (10.45), suggesting higher sensitivity of the α-glucosidase enzyme toward the phytochemical constituents of the extract within the tested concentration range. The calculated IC_{50} (Calc.IC_{50}) values for the extract and acarbose were 1069.71 and 456.24 µg/mL, respectively. The crude extract demonstrated a Potency Ratio of 0.43 relative to acarbose. Such a high relative potency (where PR > 0.1 or fold-difference < 10) is indicative of strong inhibitory activity within a crude botanical matrix.

A comparison of the maximal inhibitory capacity revealed that at a concentration of 10,000 µg/mL, the ethanolic extract achieved near-complete enzymatic blockade (92.0 %), significantly outperforming the extrapolated efficacy of acarbose (43.1%) at the same dose. This superior maximal efficacy (E_{max}) underscores the robust bioactivity of the extract's matrix.

Molecular docking *A. manihot* compounds

Molecular docking analysis was conducted to identify bioactive compounds from *A. manihot* with the potential to inhibit α-glucosidase, using acarbose as a reference ligand. Based on the docking results, the docking scores of the tested compounds ranged from –9.17 to –4.70 kcal/mol, while acarbose had a score of –7.17 kcal/mol. Since the tested compounds have a highly variable heavy-atom count (9–44 atoms), the assessment of inhibitory activity was based not only on the absolute docking score but also on ligand efficiency (LE), which quantifies the binding energy per heavy atom (Table 1).

Based on the docking results and residue interaction analysis (Fig. 1), stigmasterol, caffeic acid methyl ester, cis-p-coumaric acid, ferulic acid, hibiscone-B, and vanillic acid were selected for further investigation. Caffeic acid methyl ester (–0.41), cis-p-coumaric acid (–0.47), ferulic acid (–0.42), hibiscone-B (–0.43), and vanillic acid (–0.43) also met the LE ≤ –0.40 stringent threshold as the eligibility criterion for inhibition activity. The reference ligand acarbose is known to interact with the main catalytic residues ASP203, ASP443, and ASP542, as well as auxiliary residues THR205, TRP406, and TYR299, which play crucial roles in the catalytic activity of the enzyme (Fig. 1) (Piparo et al., 2008; Sim et al., 2008). Stigmasterol, with the lowest docking score (-9.17 kcal/mol), showed the highest binding affinity toward α-glucosidase. The interaction of this complex was dominated by hydrophobic interactions, particularly π-alkyl interactions with the TYR299, PHE575, ILE328, TRP406, and ILE364

residues. This dominance of hydrophobic interactions is consistent with the lipophilic nature of stigmasterol as a steroid, which enables stabilization of the complex through non-polar interactions within the enzyme's binding pocket. Hibiscone-B interestingly exhibits interactions similar to acarbose through the formation of conventional hydrogen bonds with ARG526, ASP203, and ASP542, key residues at the catalytic site, as well as T-shaped π-π and π-alkyl interactions with TYR299 and PHE575 (Fig. 1) (Piparo et al., 2008). This combination of polar and hydrophobic interactions provides high stability of the complex and suggests that hibiscone-B may operate via an inhibition mechanism comparable to that of acarbose. Meanwhile, vanillic acid showed a higher docking score (-5.40 kcal/mol), indicating a weaker binding affinity. This compound forms hydrogen bonds and electrostatic interactions with ARG526 and ASP327, as well as carbon-hydrogen bonds with ASP542, located around the enzyme's catalytic domain (Fig. 1). It also exhibits π-π interactions with TYR299, PHE575, TRP441, and TRP539. Further supports the hypothesis that vanillic acid can bind stably to the active site (Sim et al., 2008). Despite its LE value of –0.43, relatively high docking score (–5.1 kcal/mol), and small molecular size, which limits contact surface area with the binding pocket, vanillic acid α-glucosidase may exhibit reduced complex stability.

Conversely, cis-p-coumaric acid had the highest LE value (–0.47); however, interaction analysis showed the presence of unfavorable bonds (steric clashes) with residues ASP327, ASP366, and ASP443, which could potentially hinder optimal binding at the active site (Fig. 1). This indicates that although theoretically it has high energy efficiency, spatially the compound experiences steric hindrance that may reduce the stability of the complex. Based on docking score results, LE values, and active residue interaction analysis, hibiscone-B, vanillic acid, and stigmasterol were selected as candidate compounds with potential as α-glucosidase inhibitors. These candidate compounds were then further subjected to molecular dynamics simulations to examine the stability of their interactions at the active site of alpha-glucosidase.

Quadrant distribution and lead identification

The integration of binding affinity and atomic efficiency enabled a systematic ranking of the 27 identified compounds, distinguishing between bulky/power binders and precision fragments, using acarbose as the functional baseline (Fig. 2, Table 3). The quadrant analysis placed the clinical standard, acarbose, in a transitional zone characterized by moderate-to-high binding affinity but relatively low atomic efficiency. This positioning serves as the critical baseline for the study. Acarbose's position reflects its nature as a large, complex pseudo-tetrasaccharide. While it achieves a strong thermodynamic binding to the enzyme, which explains its clinical use, its low LE indicates that it requires a large number of atoms to exert its inhibitory effect. In this study, acarbose serves as the threshold for standard potency; any ligand appearing to the right of acarbose (higher affinity) or above it (higher efficiency) is considered a superior candidate for lead optimization. Daphniphyllin and moupinamide exhibited binding affinities nearly identical to acarbose. Their clustering suggests a similar bulky binding mechanism, in which multiple van der Waals contacts drive the interaction rather than high-precision atomic bonding.

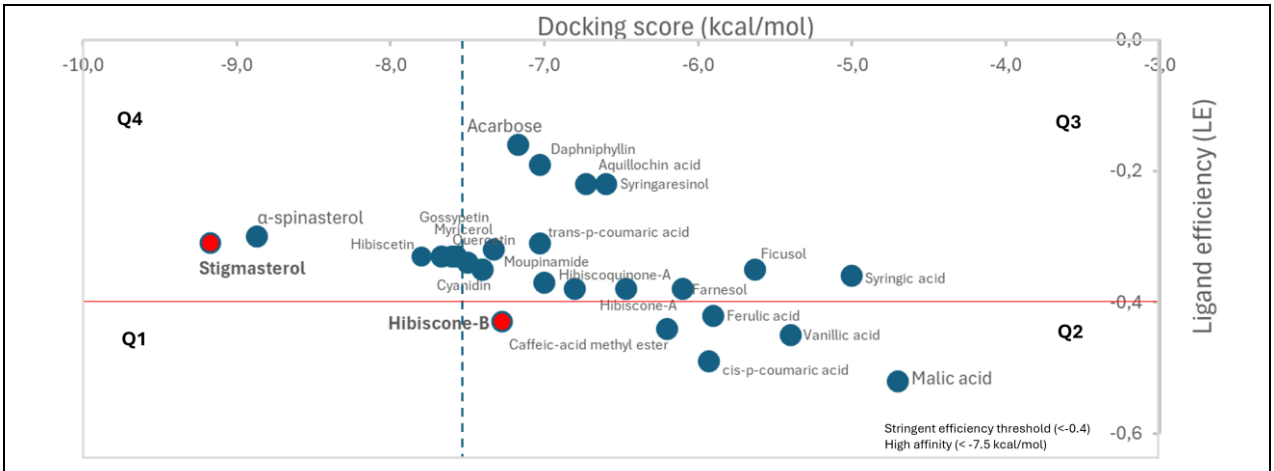


Figure 2. Bivariate distribution of binding affinity and ligand efficiency for 27 phytochemicals.

The quadrant plot employs a dual-threshold filtering strategy to prioritize drug-like candidates. The docking score of -7.5 kcal/mol represents the high-affinity boundary, identified as the upper limit for potent α-glucosidase inhibition based on the reference standard, acarbose (-7.17 kcal/mol). The ligand efficiency threshold (-0.40 kcal/mol/heavy atom) represents the stringent efficiency cutoff, as defined in medicinal chemistry, for identifying leads with optimal fit-to-size ratios. Quadrant 2 isolates precision leads like hibiscone-B, which exceed LE thresholds. Quadrant 4 categorizes power binders like stigmasterol, which exhibit superior affinity but lower structural economy. This multi-parametric filter effectively identifies molecules that offer the highest probability of persistent enzymatic blockade.

Table 3. Hierarchical prioritization of 27 phytochemicals via multi-parametric quadrant analysis.

Quadrant	Description	Rank	Ligand	Qualification
Q1 The elite performers (ΔG ≤ -7.5 and LE ≤ 0.40)	The "perfect drug": small but extremely potent		-	
Q2 The Precision Fragments (ΔG > -7.5, LE ≤ -0.4)	High efficiency (Best LE)	1	Hibiscone-B	Best overall lead
		2	Cis-p-coumaric acid	Highest atomic efficiency
		3	Vanillic acid	High stability)
		4	Caffeic acid methyl ester	Strong hydrophobic linker
		5	Ferulic acid	Balanced phenolic lead
		6	Malic acid	Fragment-like binder
Q3 The weak (ΔG > -7.5, LE > -0.4)	Low affinity/LE	1	Cyanidin	Borderline (good affinity)
		2	Kaempferol	Common flavonoid, moderate binder
		3	Moupinamide	Weakly efficient amide
		4	Hibiscoquinone-A	Moderate potency
		5	Acarbose*	Reference standard (lowest LE)
		6	Daphniphyllin	Large molecule, poor efficiency
Q4 The bulky / power binders (ΔG ≤ -7.5, LE > -0.4) and structural stability	High-affinity binders (Best LE in Q3)	1	Stigmasterol	The master binder. highest affinity; acts as a hydrophobic anchor in the enzyme cavity.
		2	α-Spinasterol	The structural peer. A highly potent phytosterol with a similar lipid-shielding mechanism to stigmasterol.
		3	Hibiscetin	The flavonoid leader. Best-performing flavonoid in terms of raw energy; bridges multiple polar sub-pockets.
		4	Gossypetin	The stable binder. High affinity with multiple hydroxyl groups for hydrogen bonding.
		5	Myricetin	The balanced binder. Solid affinity crossing the − 7.5 threshold.
		6	Myricerol	The structural bridge. A high-affinity triterpenoid that acts as a secondary hydrophobic anchor, supporting the "lipid-shield" mechanism of the phytosterols.
		7	Quercetin	The clinical peer. Exhibits a standard-strength binding profile comparable to acarbose; functions as a classical flavonoid inhibitor but lacks the "Elite" efficiency of the precision leads.

Quadrant 1 (the elite performers), notably, contained no compound, indicating that the extract's potency derives from synergistic cooperation between the precision fragments of Quadrant 2 and the power binders of Quadrant 4, rather than from a single perfect drug molecule. This distribution explains the efficacy of the crude extract: the sterols provide the initial anchoring, whereas the precision phenolics ensure a high-efficiency blockade of the catalytic center. Quadrant 2 contains the most promising drug leads. Hibiscone-B and phenolic fragments were identified as the most electronically efficient molecules. Despite having moderate raw affinity, hibiscone-B was identified as the best overall lead as its high efficiency and stability suggest a superior, precision fit. Other high-efficiency leads included Cis-p-coumaric acid, which demonstrated the highest atomic efficiency in the study, and vanillic acid. Caffeic acid methyl ester and ferulic acid also fell into this Precision category, balancing size and binding strength. Quadrant 4, the power binders, was dominated by the sterol class. Stigmasterol emerged as the master binder with the highest affinity in the study, followed closely by α-spinasterol. Although these compounds exhibited lower atomic efficiency owing to their large hydrophobic scaffolds, they function as critical hydrophobic

anchors within the enzyme cavity. While myricerol serves as a vital structural bridge within the high-affinity Quadrant 4, reinforcing the extract's bulk inhibitory capacity, quercetin was found to align closely with the acarbose baseline. This indicates that while quercetin contributes to the standard inhibitory profile, the extract's superior medicinal value is specifically driven by the more efficient leads identified in Quadrant 2.

Overall, the results of the quadrant analysis establish that the extract contains leads that are atomically more efficient than acarbose, and that hibiscone-B and stigmasterol are the candidate primary drivers of enzymatic inhibition.

Molecular dynamics (MD) simulation of *A. manihot* leaf compounds - α-glucosidase

To evaluate the dynamic stability and interaction patterns of the α-glucosidase–ligand complex, a 100 ns molecular dynamics (MD) simulation was performed. MD simulation was performed on acarbose as the reference standard, stigmasterol as the power binder lead, hibiscone-B as the precision lead, and vanillic acid as the comparator lead. The parameters analyzed included the root-mean-square deviation (RMSD) to assess the stability of the complex relative to the protein backbone, and the number of hydrogen bonds (H-bonds) to assess the contribution of non-covalent interactions to the complex's stability during the simulation. The RMSF was calculated to evaluate the local flexibility of individual amino acid residues. This ensures that the ligand-binding event effectively stabilizes the catalytic domain, reducing the vibrational noise that would otherwise interfere with enzymatic inhibition. Complete results for MD of hibiscone-B and vanillic acid complex with α-glucosidase were uploaded (https://doi.org/10.5281/zenodo.18124023).

The RMSD profiles (Fig. 3A) highlight that the α-glucosidase— acarbose complex (reference ligand) exhibits a stable RMSD throughout 100 ns, with minor fluctuations in the range of 10–11 Å. This stability indicates that acarbose maintains a strong and consistent binding orientation at the enzyme's active site, consistent with its experimentally proven role as an α-glucosidase inhibitor. The α-glucosidase—hibiscone-B complex exhibited a multi-phase stabilization profile. Following initial fluctuations (0–12 ns), the complex reached a steady plateau between 12 and 45 ns, with an average RMSD of 8–9 Å. A transient conformational shift was observed between 45 and 60 ns (6–15 Å), after which the system re-stabilized and maintained a consistent plateau of 8–9 Å from 60 to 95 ns. This pattern illustrates a phase in which the ligand undergoes conformational adjustments, exploring different subpockets within the large MGAM active site before relocking into a stable pose at the enzyme's active site. In contrast, the α-glucosidase–vanillic acid complex experiences greater fluctuations (5–15 Å) in the early stages (0–40 ns), but these gradually decrease and achieve stability during the latter stages, with RMSD values of approximately 6 Å (Fig. 3A). Vanillic acid follows a settling pattern. The high initial fluctuations suggest it takes time to find its optimal orientation, but its low final RMSD suggests a very tight, compact fit once settled. Vanillic acid, small in size, is able to maintain a stable binding position relative to the enzyme backbone, indicating a favorable binding orientation within the active pocket.

The flexibility of protein residues during molecular dynamics simulations was analyzed using RMSF calculations. In general, most protein residues showed low RMSF values, confirming the stability of the protein structure throughout the simulation (Fig 3B). Increased fluctuations were generally observed in the loop regions and terminal ends of the protein, which inherently exhibit higher mobility. showed relatively low RMSF values. The catalytic pocket residues maintained RMSF values below 0.15 nm, significantly lower than the global protein average of ~0.25–0.30 nm. Residues directly involved in ligand interactions, including ARG526, ASP542, TYR299, and TRP406, exhibited high structural rigidity (< 0.1 nm) upon binding, indicating that the binding pocket region remained stable and maintained crucial interactions with the ligand throughout the simulation.

Acarbose and stigmasterol consistently showed the greatest reductions in peak intensities. While acarbose effectively stabilized the central region, stigmasterol excels at minimizing fluctuations in the hydrophobic regions. This characteristic accounts for the notably high van der Waals energy observed in the MM-PBSA analysis, as stigmasterol occupied the binding pocket like a plug. Hibiscone-B was very stable in the active site, whereas it exhibited greater fluctuations in flexible loop regions (the sharp peak near residues 380 and 800 in Fig. 3B). This indicates that hibiscone-B is a precision inhibitor; it locks the active site while allowing the rest of the protein to remain dynamic. Vanillic acid exhibited the greatest overall fluctuations across the protein backbone. It was bound to the enzyme but did not lock it, suggesting a role as an auxiliary stabilizer rather than a primary inhibitor.

Analysis of the number of hydrogen bonds (Fig. 3C) supports the RMSD results, as the stability of a complex generally correlates positively with the presence of consistent hydrogen bonds. The acarbose complex formed a high and stable number of hydrogen bonds throughout the simulation, likely involving key catalytic residues such as ASP542, ASP443, and ASP203.

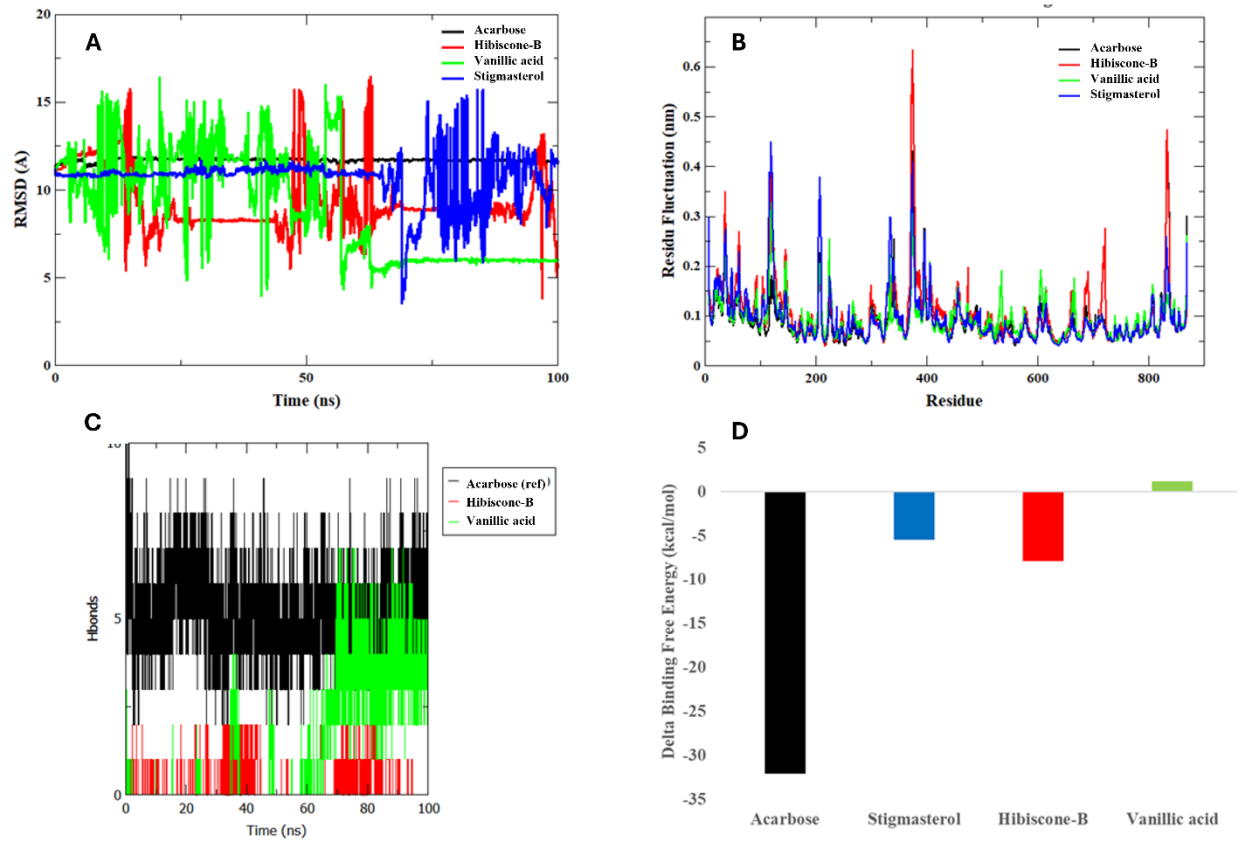


Figure 3. Structural stability and flexibility of selected lead complexes.

(A) Dynamic stability as root mean square deviation (RMSD) profile of candidate ligand–α-glucosidase complexes over a 100 ns trajectory. This illustrates the structural equilibration of hibiscone B and stigmasterol relative to acarbose. **(B)** Root mean square fluctuation (RMSF) profile candidate complexes on α-glucosidase backbone residues. **(C)** The number of bonds formed at the active site of α-glucosidase, highlighting the electrostatic network maintained by the lead molecules compared to acarbose during the simulation. **(D)** Comparison of ΔGtotal that reflects the true affinity of the lead compounds in a biological system.

Table 4. Deconvolution of MM-PBSA binding free energy components.

Compound	ΔEvdw (kcal/mol)	ΔEelec (kcal/mol)	ΔGsolv (kcal/mol)*	ΔGtotal (kcal/mol)	Primary driving force
Acarbose	-12.45	-85.30	+65.67	-32.08	Electrostatic/polar
Hibiscone B	-18.24	-4.15	+14.47	-7.92	van der Waals (hydrophobic)
Stigmasterol	-21.10	-0.85	+16.48	-5.47	van der Waals (lipophilic)
Vanillic acid	-5.12	-3.45	+9.73	+1.16	Unfavorable (desolvation penalty)

The persistence of these bonds indicates a significant contribution of electrostatic interactions to the stability of the complex. Hibiscone-B forms a combination of π interactions and hydrogen bonds with residues such as TRP406 and PHE575, and several persistent hydrogen bonds mainly with the ASP203 and ASP542 residues. The more flexible π-π stacking or π-alkyl interaction allowed hibiscone-B to breathe in the pocket without dissociating.

Although the number of H-bonds was slightly lower than that of acarbose, their consistency throughout the simulation, together with these π interactions, plays an important role in maintaining the stability of the complex conformation once equilibration is achieved. vanillic acid, which has a smaller molecular size, forms two to three stable hydrogen bonds with the ASP327 and ASP542 residues. The persistence of these bonds, particularly in the 60–100 ns timeframe, explains the better RMSD conformational stability in the later phase of the simulation.

To provide a rigorous thermodynamic profile of the binding event, MM-PBSA was employed. Unlike grid-based scoring, MM-PBSA accounts for the solvent effect and polar/non-polar contributions, providing a

quantitative binding free energy (ΔG) that reflects the true affinity of the lead compounds in a biological system. The calculated results show that acarbose, the positive control, has a total binding energy of −32.08 kcal/mol, indicating a significant contribution from electrostatic interactions with the enzyme (Fig. 3D, Table 4). Among the candidate compounds, hibiscone-B exhibited the most favorable binding free energy (ΔGtotal = −7.92 kcal/mol), followed by stigmasterol (−5.47 kcal/mol). Conversely, Vanillic acid showed a positive binding energy value (1.16 kcal/mol), indicating a less stable interaction. The energy component analysis revealed that the energy contributions in hibiscone-B and stigmasterol were dominated by van der Waals interactions, whereas the strong electrostatic interactions observed in acarbose correlated with the high density of polar groups in its structure.

In summary, the integration of molecular docking results, molecular dynamics simulations, and MM-PBSA analysis indicated that hibiscone-B and stigmasterol showed greater potential as α-glucosidase inhibitors than vanillic acid. Hibiscone-B shows an optimal balance between polar and hydrophobic interactions, resulting in good complex stability during simulations and a relatively stable binding energy. Stigmasterol, in contrast, exhibits strong binding affinity, primarily mediated by hydrophobic interactions. Vanillic acid, however, displays lower interaction stability, possibly due to its limited molecular size and smaller contact surface area with the enzyme's active site. Despite the slightly positive global ΔG calculated over the total trajectory, the stabilization of H-bonds with ASP542 in the latter 40 ns suggests a transient or concentration-dependent inhibitory potential for vanillic acid.

DISCUSSION

In this study, the observed disparity in the required concentration between the ethanolic extract of *A. manihot* leaves and acarbose was anticipated. Acarbose is a singular active pharmaceutical ingredient, whereas the extract comprises a mixture of compounds. Consequently, this difference in IC_{50} between acarbose and the extract can be attributed to differences in the potency of the active compounds and the proportion of each potent α-glucosidase inhibitor in the extract. Within the extract, different phytochemicals may compete for the same binding site or interact with one another (forming complexes) before reaching the enzyme, thereby reducing their effective concentrations. Furthermore, the dilution of the extract, particularly for high-potency ligands (such as α-spinasterol or cis-p-coumaric acid), which may constitute only 1% to 5% of the total mass, resulted in elevated IC_{50} values. While stigmasterol blocks one side and vanillic acid hits the center, they may interfere with each other (competitive inhibition) or may not be present at sufficiently high concentrations to saturate all enzyme molecules. In an *in vitro* assay, the enzyme and inhibitors are in constant contact. Smaller plant compounds are more slippery and may bind more slowly, resulting in a higher measured IC_{50} in the crude extract. The RMSD data indicated that hibiscone-B and vanillic acid require 30–40 ns to achieve stable poses. In contrast, pure acarbose, being a substantial molecule, binds to the enzyme almost immediately.

Interestingly, although acarbose demonstrated a lower IC_{50}, the ethanolic extract of *A. manihot* exhibited superior maximum efficacy. At a concentration of 10,000 µg/mL, the extract achieved 92.0% inhibition, whereas acarbose was extrapolated to reach only 43.1%. Thus, the crude *A. manihot* extract was 2.13 times more effective than acarbose at this dose. This suggests that while acarbose is potent at microdoses, the phytochemical complex within the extract provides a more complete enzymatic blockade at higher concentrations. In pharmacology, this is known as potency (IC_{50}) versus efficacy (E_{max}). The regression models support the notion that the flat acarbose response curve (slope = 10.45) suggests that, at a certain level, adding more acarbose does not increase inhibition.

In contrast, the steep curve of the extract (slope = 46.60) indicates that the inhibitory power increases rapidly with increasing dose. In a clinical setting, this suggests that for patients with very high postprandial glucose spikes, the extract might provide a stronger ceiling of protection than acarbose. The high E_{max} of the extract is likely attributed to the synergistic effect of bulky hydrophobic binders, such as stigmasterol, which was identified in the docking study as having superior affinity compared to acarbose.

The docking and quadrant analyses identified hibiscone-B as a precision lead due to its superior ligand efficiency (LE = −0.43) and stable binding mode. According to Ndarawit et al. (2024), the stability of a complex is determined by whether the ligand remains in the active site and if the RMSD reaches a plateau (a steady state). Molecular dynamics simulations of leads, vanillic acid, and hibiscone-B, revealed distinct binding behaviors. The acarbose standard demonstrated the most consistent stability across the 100 ns trajectory, with a mean RMSD of 11 Å. The relatively higher absolute RMSD of acarbose compared to vanillic acid and hibiscone-B is consistent with observations by Ndarawit et al. (2024), who reported that larger, flexible molecules often exhibit higher displacement values while maintaining a stable binding envelope within the protein matrix.

In contrast, the vanillic acid complex displayed significantly higher early-stage mobility (0–40 ns, 5–15 Å);

it eventually achieved a highly compact and stable state from 60 to 100 ns with a mean RMSD of 6 Å. The high initial fluctuation is typical for smaller phenolic structures exploring the active site. Its small molecular size may not adequately occupy the catalytic pocket, which aligns with its lower experimental inhibition potency (PR = 0.10). Derivatives of vanillic acid synthesized by others have consistently demonstrated lower inhibition rates than acarbose (Wang et al., 2025). Compared with vanillic acid, hibiscone-B has been identified as a superior lead compound. Hibiscone-B demonstrated a dynamic stability profile and periodic fluctuations that re-stabilized at 8–9 Å after a brief conformational shift at 45–60 ns. Such re-stabilization events suggest that the ligand undergoes a conformational adjustment to optimize its fit within the expansive catalytic cleft of MGAM (Ndarawit et al., 2024). Hibiscone-B maintained a robust binding conformation characterized by a low RMSD, indicating that its inhibitory activity is supported by a stable and biologically pertinent interaction with critical catalytic residues. The ability of hibiscone-B to maintain a stable plateau for the majority of the simulation—with a final RMSD lower than that of the acarbose standard (11 Å)—corroborates its superior *in vitro* potency (PR = 1.51). The bivariate quadrant analysis prioritized stigmasterol as a high-affinity lead, as it exhibits a hydrophobic profile, high ligand efficiency (LE), and a favorable geometric fit within the enzyme's entrance channel. In the quadrant analysis, stigmasterol mapped closely to the potency threshold of acarbose but showed a more favorable binding energy-to-atom ratio. This suggests that its inhibition is not due to nonspecific aggregation but rather to a highly optimized van der Waals interaction with the hydrophobic subpockets of α-glucosidase. In terms of ΔG, when lipophilic molecules enter the enzyme pocket, they push out trapped water molecules. This increase in the entropy of the water (+ΔS) makes the overall binding energy (ΔG) much more favorably negative.

To further discuss the inhibitory potential of the identified phytochemicals, a comparative analysis was performed using a secondary literature dataset. A comparative analysis, using potency ratios normalized to their respective acarbose standards, was conducted to benchmark the *A. manihot* ethanolic extract against its pure metabolites. An *in vitro* inhibition assay (Hajra et al., 2024) reported that pure stigmasterol is 2.1 times more potent than acarbose. This is in accordance with our docking results, in which stigmaterol (-9.17 kcal/mol) was stronger than acarbose (-7.17 kcal/mol). Thus, reinforces the conclusion that the presence of these potent phytosterols significantly drives the high maximal inhibition (92.0%) observed in this study. The inhibition assay of hibiscone B isolated from *A. moschatus* subsp. *Tuberosus* exhibits a PR of 1.51 (Dung et al., 2021). This also aligns with the multi-parametric *in silico* profile. Specifically, hibiscone-B RMSD stability (8–9 Å) indicates a more rigid occupancy of the catalytic cleft than the acarbose standard (11 Å). This structural stability is driven by precision atomic interactions with the catalytic residues Asp442 and Asp571, resulting in a favorable LE (LE = -0.43). The ability of hibiscone-B to maintain a stable plateau for the majority of the simulation—with a final RMSD lower than the acarbose standard (11 Å)—corroborates its superior *in vitro* potency PR = 1.51. Other *in vitro* assays revealed PR of phenolic phytochemicals ferulic acid (0.355), p-coumaric acid (0.157), vanillic acid (0.113), and syringic acid (0.098) (Aleixandre et al., 2022). The ranking of potency ratios (ferulic > vanillic > syringic acid) showed a perfect correlation with the *in silico* docking affinities (-5.90 > -5.40 > -5.00 kcal/mol). This correlation empirically validates the predictive accuracy of the docking model. These results also suggest that the high maximum inhibition (92%) of the extract is a cumulative effect of highly potent compounds, such as stigmasterol, hibiscone-B, working alongside efficient phenolic scaffolds.

The efficiency of the botanical matrix can be seen from dual benchmarking, i.e., the potency of the *A. manihot* extract was compared to two distinct tiers of phytochemical leads, precision fragment leads (hibiscone-B), and power binder/high-affinity leads (stigmasterol) using normalized potency ratios (PR) from this study (extract) and literature (pure form of leads). Firstly, the crude extract's PR (0.43) was compared to hibiscone-B PR (1.51), resulting in a 3.5-fold difference in efficacy, which is remarkably narrow for a non-fractionated extract. Comparison of the crude extract and stigmasterol (PR = 2.1) revealed a 5-fold potency gap, indicating an exceptionally high concentration of potent metabolites in the plant matrix. Usually, a crude extract is 100× to 1000× weaker than a pure compound. In line with the logic of synergistic phytochemistry, this suggests that the extract's inhibitory power derives from a high concentration of active metabolites or from synergistic interactions among its diverse chemical constituents, effectively bridging the gap between crude mixtures and pure pharmaceutical standards. Secondly, the extract demonstrated a higher relative potency than several pure precision fragments, leading specifically outperforming ferulic acid (0.355), p-coumaric acid (0.157), vanillic acid (0.113), and syringic acid (0.098). Following the principles of ethnopharmacology, this crude-over-pure superiority provides empirical evidence of synergistic interactions in which minor phenolic constituents enhance the overall enzymatic blockade. This dual benchmarking validation—alignment with high-affinity binders and superiority over precision fragments—solidifies the extract as a robust candidate for standardized anti-diabetic therapy.

The functional synergy phenomenon is when a botanical matrix achieves high-efficacy enzymatic inhibition through the simultaneous interaction of structurally diverse ligands with multiple sub-sites within a single catalytic domain, resulting in a persistent blockade that exceeds the calculated additive effect of isolated components. Such synergy is likely characterized by (1) kinetic cooperativity, (2) physicochemical synergy (solubility and bioavailability), and (3) structural economy (atomic efficiency). In kinetic cooperativity, the synergy of the *A. manihot* leaf extract is structurally underpinned by a dual-site blockade of the α-glucosidase pocket. The MD simulations reveal that while the reference standard, acarbose, relies on a high-density electrostatic network with ASP443 and ASP203, the prioritized phytochemical leads utilize distinct, non-overlapping residues. Hibiscone-B achieves stability through persistent π-interactions with TRP406 and PHE575, coupled with targeted hydrogen bonding at ASP542. Simultaneously, the larger stigmasterol molecule provides a hydrophobic anchoring effect, stabilized by van der Waals interactions within the peripheral regions. The relative immobilization of ARG526 and TYR299 (low RMSF) further suggests that these leads effectively lock the flexible loop regions, preventing the conformational changes necessary for substrate processing. This tag-team occupancy ensures that the active site remains obstructed across a broader range of conformational states than a single purified inhibitor could achieve. Such multi-residue engagement also explains how the phytochemical matrix maintains high inhibitory efficacy (92%) by obstructing both the catalytic dyad and the auxiliary substrate-binding subsites. Consequently, the extract bridges the potency gap relative to acarbose not through a single lead molecule, but through a multi-scaffold synergistic pressure that maximizes enzymatic blockade while minimizing the concentration required for any individual constituent.

The physicochemical synergy relates to the solubility and availability of the compounds. In an *in vitro* assay, pure compounds often struggle with solubility. In a crude extract, the presence of various matrix compounds can act as natural surfactants, keeping hydrophobic leads like stigmasterol more available to interact with the enzyme than they would be in a purified, isolated state. Our LC-ESI-MS profiling of *A. manihot* extract (Tangka et al, 2021) and other data (Winata et al., 2024) reveal a significant steroid-to-flavonoid ratio (approximately 4:1). While steroids represent the largest chemical fraction (93.992 mg/g), their high lipophilicity typically presents a thermodynamic barrier to enzymatic binding, as reflected in the positive desolvation energies (ΔGsolv) observed in MM-PBSA models. The substantial flavonoid glycosides (e.g., kaempferitrin, quercetin-3-O-rutinoside, myricetin-3-O-beta-D-glucopyranoside, hibiscetin-3-glucoside) content (23.337 mg/g) serves as a natural surfactant system. The amphiphilic molecules likely form a solvation shell around the high-affinity but poorly water-soluble leads such as stigmasterol and hibiscone B, effectively carrying them into the α-glucosidase active site. For instance (but not limited to), the synergistic surfactant-lead pairs of kaempferitrin—stigmasterol and hibiscetin-3-glucoside—hibiscone B. Kaempferitrin, a large, bulky glycoside, can readily shield the rigid sterol structure. The amphiphilic hibiscetin-3-glucoside helps hibiscone-B through its flat, aromatic part aglycone (hibiscetin), which sticks to the flat rings of hibiscone-B via π-π stacking, and through its glucose moiety, which points outward toward the water, creating a hydration shell for hibiscone-B. Such matrix-mediated solubility prevents the aggregation of high-affinity lipophilic binders—a synergistic advantage often lost upon purification. This explains why the crude extract achieves a potent IC_{50} despite the hydrophobic nature of its primary constituents. Once delivered, the steroids capitalize on their high van der Waals complementarity (ΔEvdw: -21.10 kcal/mol), providing a stable, low-entropy blockade that outperforms the clinical standard, acarbose, in terms of atomic efficiency.

The concept of synergy through structural economy, also known as atomic efficiency, is also exemplified by hibiscetin-3-glucoside, a single molecule capable of performing two distinct functions. Firstly, it lowers the desolvation penalty by interacting with water molecules, making it easier for the actual cargo (stigmasterol or hibiscone-B) to enter the α-glucosidase pocket. Utilizing its extensive polyhydroxyl network, it anchors the entrance of the catalytic pocket via strong electrostatic interactions (ΔEelec). The high ΔEelec relative to their small size, meaning every atom is working to pull the molecule into the pocket (atomic efficiency). This polar stabilization complements the massive van der Waals contribution of the steroid fraction. Specifically, while stigmasterol rigidifies the inner hydrophobic subpockets (RMSF < 0.15 nm), hibiscetin-3-glucoside enhances the bioavailability of these lipophilic leads by acting as a high-efficiency natural surfactant. Secondly, it acts as a competitive inhibitor by mimicking the natural substrate of α-glucosidase, tricking the enzyme into binding to it rather than to starch. Another example illustrating structural economy is the synergy between vanillic acid and stigmasterol. While stigmasterol blocks the main channel, vanillic acid fills the side-pockets, creating a multi-site blockade. Because vanillic acid is a small phenolic, it can fit into a narrow space that acarbose is too bulky to enter. Thus, the extract achieves complete blockade using two smaller, simpler molecules rather than a single massive, complex one.

CONCLUSION

This study successfully characterized the anti-diabetic potential of *A. manihot* by bridging the gap between crude extract efficacy and molecular-level interactions. Through the triangulation of experimental IC_{50} data, 100 ns molecular dynamics simulations, and comparative analysis with existing literature, it established a robust profile for *A. manihot* as a potent source of α-glucosidase inhibitors. The hibiscone-B and stigmasterol were identified as high-affinity leads. Their biological efficiency (PR > 1.0), structural stability and flexibility, and their rigidification of the catalytic dyad (Asp442/Asp571) during 100 ns simulations confirm their role as the primary drivers of enzymatic blockade. The dual benchmarking found that the extract's potency is not merely a function of individual constituents but a result of a synergistic matrix that outperforms several pure phenolic standards. Furthermore, the complex metabolite profile—characterized by a strategic 4:1 ratio of glycoside surfactants to lipophilic leads—suggests a natural micellar delivery system that maintains lead bioavailability in aqueous environments. These findings position its constituent phytochemicals as high-efficiency scaffolds for the development of next-generation, non-sugar-based α-glucosidase inhibitors. Ultimately, the 2.34-fold potency gap between the crude extract and the pure drug acarbose underscores the *A. manihot* viability as a source for standardized phytomedicines. The implication of the finding that a crude extract outperforms pure (phyto)chemicals shifts the focus from single-molecule drugs to standardized-extract therapies. Future studies should focus on the *in vivo* pharmacokinetic validation of these prioritized leads to confirm their systemic efficacy.

CONFLICT OF INTEREST

The research was conducted entirely free from any involvement in commercial, financial, or personal matters that might be perceived as a possible conflict of interest or that could have influenced the outcomes or interpretation of the study.

ACKNOWLEDGMENTS

The authors would like to thank Dr. Didik Widyatmoko from the Center for Plant Conservation, Botanic Gardens – Indonesia Institute of Sciences, Bogor, Indonesia, for the determination of the *A. manihot* leaves, and Fitri Armania from the Laboratory of Biomedical Science at the Faculty of Medicine of Universitas Brawijaya for enabling the *in vitro* works done. This research did not receive any specific grant from funding agencies in the public, commercial, or not-for-profit sectors.

GENERATIVE ARTIFICIAL INTELLIGENCE (AI)

The authors used Paperpal (paperpal.ai) to improve the language and readability of the manuscript. The authors reviewed and edited the content and take full responsibility for its accuracy. No images were generated or manipulated using AI tools.

REFERENCES

Abad-Zapatero C, Metz JT (2005) Ligand efficiency indices as guideposts for drug discovery. Drug Discov Today 10(7): 464–469. https://doi.org/10.1016/S1359-6446(05)03386-6

Abraham MJ, Murtola T, Schulz R, Páll S, Smith JC, Hess B, Lindahl E (2015) GROMACS: High performance molecular simulations through multi-level parallelism from laptops to supercomputers. SoftwareX 1–2: 19–25. https://doi.org/10.1016/j.softx.2015.06.001

Agu PC, Afiukwa CA, Orji OU, Ezeh EM, Ofoke IH, Ogbu CO, Ugwuja EI, Aja PM (2023) Molecular docking as a tool for the discovery of molecular targets of nutraceuticals in diseases management. Sci Rep 13(1): 13398. https://doi.org/10.1038/s41598-023-40160-2

Aleixandre A, Gil JV, Sineiro J, Rosell CM (2022) Understanding phenolic acids inhibition of α-amylase and α-glucosidase and influence of reaction conditions, Food Chem 372: 131231. https://doi.org/10.1016/j.foodchem.2021.131231

Cole DJ, Horton JT, Nelson L, Kurdekar V (2019) The future of force fields in computer-aided drug design. Future Med Chem 11(18): 2359–2363. https://doi.org/10.4155/fmc-2019-0196

Dassault S (2020) BIOVIA Discovery Studio Visualizer, v20.1. San Diego: Dassault Systèmes.

DeFronzo RA, Ferrannini E, Groop L, Henry RR, Herman WH, Holst JJ, Hu FB, Kahn CR, Raz I, Shulman GI, Simonson DC, Testa MA, Weiss R (2015) Type 2 diabetes mellitus. Nat Rev Dis Primers 1(1): 15019. https://doi.org/10.1038/nrdp.2015.19

Dung HV, Anh PT, Hoa HQ, Dung DT, Tai BH, Kiem PV, Than DT, Thao DT, Nhien NX, Quyen D (2021) Two new cadinane sesquiterpenes and one new lignan from *Abelmoschus moschatus* subsp. tuberosus and their α-glucosidase inhibitory activity. Phytochem Lett 41: 1–5. https://doi.org/10.1016/j.phytol.2020.10.013

Finney DJ (1978) Statistical Method in Biological Assay. 3. ed. Charles Griffin & Co., London and High Wycombe VII, 508 S.

Fisher M (2022) Acarbose and alpha glucosidase inhibitors. In: Fisher M, Mckay GA, Llano A (eds), Diabetes Drug Notes, pp. 229–238. https://doi.org/10.1002/9781119785033.ch11

Fitriyah NYA, Tangka J, Amalia Y, Purnomo Y (2020) Effect of ethanolic extract of *Abelmoschus manihot* (L.) Medik on tissue TNF-alfa levels and aortic lumen diameter of diabetic rat. J Comm Med 8 (2): 1–7.

Fuadi A, Tangka J, Martino YA, Purnomo Y (2020) Potency of ethanolic extract of *Abelmoschus manihot* (L.) Medik on kidney SOD levels and kidney MDA levels in diabetic rat model. J Bio Kompl Med 7(2): 1–8.

Genheden S, Ryde U (2015) The MM/PBSA and MM/GBSA methods to estimate ligand-binding affinities. Expert Opin Drug Discov 10(5): 449–461. https://doi.org/10.1517/17460441.2015.1032936

Guo Z, Niu X, Xiao T, Lu J, Li W, Zhao Y (2015) Chemical profile and inhibition of α-glycosidase and protein tyrosine phosphatase 1B (PTP1B) activities by flavonoids from licorice (*Glycyrrhiza uralensis* Fisch). J Func Foods 14: 324–336. https://doi.org/10.1016/j.jff.2014.12.003

Gupta P, Bala M, Gupta S, Dua A, Dabur R, Injeti E, Mittal A (2016) Efficacy and risk profile of anti-diabetic therapies: Conventional vs traditional drugs—A mechanistic revisit to understand their mode of action. Pharmacol Res 113: 636–674. https://doi.org/10.1016/j.phrs.2016.09.029

Hajra D, Chouni A, Paul S (2024) Phytochemistry, antioxidant and anti-diabetic activities of *Sterculia villosa* in-vitro, Pharmacol Res - Mod Chin Med 13: 100530. https://doi.org/10.1016/j.prmcm.2024.100530

Hamza AA, Ksiksi TS, Shamsi OAA, Balfaqh SA (2015) α-Glucosidase inhibitory activity of common traditional medicinal plants used for diabetes mellitus. J Dev Drugs 4(5): 1–5.

Hanwell MD, Curtis DE, Lonie DC, Vandermeersch T, Zurek E, Hutchison GR (2012) Avogadro: An advanced semantic chemical editor, visualization, and analysis platform. J Cheminform 4(1): 17. https://doi.org/10.1186/1758-2946-4-17

Hopkins AL, Groom CR, Alex A (2004) Ligand efficiency: A useful metric for lead selection. Drug Discov Today 9(10): 430–431. https://doi.org/10.1016/S1359-6446(04)03069-7

Huang J, MacKerell AD Jr (2013) CHARMM36 all-atom additive protein force field: Validation based on comparison to NMR data. J Comput Chem. 34(25): 2135–2145. https://doi.org/10.1002/jcc.23354

Hubbard RE, Haider MK (2010) Hydrogen bonds in proteins: Role and strength. eLS. https://doi.org/10.1002/9780470015902.a0003011.pub2

Khan MAB, Hashim MJ, King JK, Govender RD, Mustafa H, Al Kaabi J (2020) Epidemiology of type 2 diabetes - global burden of disease and forecasted trends. J Epidemiol Glob Health 10(1): 107–111. https://doi.org/10.2991/jegh.k.191028.001

Kumari R, Kumar R, Lynn A (2014) g_mmpbsa—A GROMACS tool for high-throughput MM-PBSA calculations. J Chem Inf Model 54(7): 1951–1962. https://doi.org/10.1021/ci500020m

Ndarawit W, Ochieng CO, Angwenyi D, Cruz JN, Santos CBR, Kimani NM (2024) Discovery of α-amylase and α-glucosidase dual inhibitors from NPASS database for management of type 2 diabetes mellitus: A chemoinformatic approach. PLoS ONE 19(11): e0313758. https://doi.org/10.1371/journal.pone.0313758

Nurasidah R, Tangka J, Elyani H, Purnomo Y (2020) Effect ethanolic extract of *Abelmoschus manihot* (L.) Medik on renal tumor necrosis factor alpha (TNF-α) levels and glomerular epithelial cell necrosis levels in diabetic rat model. J Bio Kompl Med 7 (2): 1–10.

Nurrani L, Kinho J (2013) Utilization of natural plant by the North Sulawesi community as a lowering of diabetic. International Conference on Forest and Biodiversity, Manado Forestry Research Institute, Manado, Indonesia, July 5, pp 443–452.

Piparo LE, Scheib H, Frei N, Williamson G, Grigorov M, Chou CJ (2008) Flavonoids for controlling starch digestion: Structural requirements for inhibiting human α-amylase. J Med Chem 51(12): 3555–3561. https://doi.org/10.1021/jm800115x

Sakinah A, Tangka J, Purwanti S, Purnomo Y (2020) Effect of ethanol extract of *Abelmoschus manihot* (L.) Medik on TNFalfa heart levels and total of cardiomyocyte necrosis in diabetes mellitus rats. J Bio Kompl Med 7 (2): 1–9.

Sim L, Quezada-Calvillo R, Sterchi EE, Nichols BL, Rose DR (2008) Human intestinal maltase–glucoamylase: crystal structure of the N-terminal catalytic subunit and basis of inhibition and substrate specificity. J Mol Biol 375(3): 782–792. https://doi.org/10.1016/j.jmb.2007.10.069

Suoth E, Kaempe H, Tampi A (2013) Evaluation of total polyphenol and flavonoids isolation of red gedi leaves (*Abelmoschus manihot* L.) (Evaluasi Kandungan Total Polifenol dan Isolasi Senyawa Flavonoid Pada Daun Gedi Merah) Chem Prog 6(2): 86–91. https://doi.org/10.35799/cp.6.2.2013.3500

Tangka J, Barung EN, Lyrawati D, Soeatmadji D, Nurdiana N (2022) DPP-IV inhibitory activity of the ethanolic extract of red gedi leaves *Abelmoschus manihot* L. Medic. Open Access Maced J Med Sci 10(A): 207–213. https://doi.org/10.3889/OAMJMS.2022.8356

Tangka J, Barung EN, Lyrawati D, Soeatmadji DW, Nurdiana (2021) Identification of metabolite compounds from ethanolic extract of the red gedi leaves (abelmoschus manihot L. Medik) by LC-ESI-MS. Res J Pharm Tech 15(11): 5164–5167. https://doi.org/10.52711/0974-360X.2022.00869

Trott O, Olson AJ (2010) AutoDock Vina: Improving the speed and accuracy of docking with a new scoring function, efficient optimization, and multithreading. J Comput Chem 31(2): 455–461. https://doi.org/10.1002/jcc.21334

Van Der Spoel D, Lindahl E, Hess B, Groenhof G, Mark AE, Berendsen HJ (2005) GROMACS: Fast, flexible, and free. J Comput Chem 26(16): 1701–1718. https://doi.org/10.1002/jcc.20291

Vanommeslaeghe K, Raman EP, MacKerell AD Jr (2012) Automation of the CHARMM General Force Field (CGenFF) II: Assignment of bonded parameters and partial atomic charges. J Chem Inf Model 52(12): 3155–3168. https://doi.org/10.1021/ci3003649

Wang D, Wu Y, Pan W, Zhang Y, Wang X, Li P (2025) Design, synthesis, and bioactivity evaluation of novel vanillic acid derivatives containing an 1,2,4-triazole thioether moiety. Russ J Gen Chem 95: 3405–3411. https://doi.org/10.1134/S1070363225605009

Winata GM, Hardiansyah H, Marliyati SA, Rimbawan R, Andrianto D (2024) Phytochemical compounds and antioxidant capacities of *Abelmoschus manihot* leaf extracts using different solvents. Biodiversitas 25(3): 942–949. https://doi.org/10.13057/biodiv/d250305

AUTHOR CONTRIBUTION:

Contribution	Tangka J	Dumanauw JM	Nurdiana	Salam R	Lyrawati D
Concepts or ideas	x	x	x	x	x
Design	x	x	x	x	x
Definition of intellectual content	x	x	x	x	x
Literature search	x			x	x
Experimental studies	x	x	x		x
Data acquisition	x				x
Data analysis	x			x	x
Statistical analysis	x			x	x
Manuscript preparation	x	x	x	x	x
Manuscript editing	x	x	x	x	x
Manuscript review	x	x	x	x	x

Citation Format: Tangka J, Dumanauw JM, Nurdiana, Salam R, Lyrawati D (2026) Identifying high-efficiency α-glucosidase inhibitors from *Abelmoschus manihot* (L.) Medik.: A quadrant-based integration of *in vitro* potency and *in silico* analysis. J Pharm Pharmacogn Res 14(2): 2272. https://doi.org/10.56499/jppres_14.2.2272

Publisher's Note: All claims expressed in this article are solely those of the authors and do not necessarily represent those of their affiliated organizations, or those of the publisher, the editors and the reviewers. Any product that may be evaluated in this article, or claim that may be made by its manufacturer, is not guaranteed or endorsed by the publisher.

Open Access: This article is distributed under the terms of the Creative Commons Attribution 4.0 International License (http://creativecommons.org/ licenses/by/4.0/), which permits use, duplication, adaptation, distribution and reproduction in any medium or format, as long as you give appropriate credit to the original author(s) and the source, provide a link to the Creative Commons license and indicate if changes were made.